


DUAL ESTIMATION OF IRON OXIDE DEPOSITION ON DRINKING WATER PVC PIPES USING CALIBRATED TURBIDITY DATA AND BRIGHTFIELD MICROSCOPY IN A FULL-SCALE LABORATORY SYSTEM

Artur Sass Braga ¹ and Yves Filion ²

^{1,2}Queen's University
Kingston, Ontario, (Canada)

¹  16asb2@queensu.ca, ² yves.filion@queensu.ca

Abstract

The assessment of accumulated sediments inside drinking water pipes is an important step for determining the risk of water quality deterioration for a sector of a distribution network and for scheduling the required maintenance activities that minimize this risk. Water utilities and researchers have traditionally used turbidity data collected during flushing operations to quantify the discolouration potential in isolated pipe lengths. Flushing has an elevated cost of specialized personnel, consumes large quantities of drinking water, and offers poor information about sediment conditions prior to mobilization (e.g. structure, position on the pipes). The last problem must be overcome by gaining a better understanding of the processes driving material accumulation, which might help in the development of strategies to prevent sediment deposits. In addition, a complex relationship between turbidity and SSC also makes it difficult to accurately translate turbidity units (NTU) into physical units of concentration (e.g. mg/L). This paper aims to consolidate the macroscopic estimations of sediment deposits in drinking water pipes using turbidity data and to propose a microscopic complement that provides richer data about sediment deposits at the pipe wall. The research was developed through a controlled experiment using a full-scale PVC pipe system that mimics the operational conditions of drinking water distribution systems. In the experiments, the drinking water was amended with iron oxide particles that progressively adhered to the pipe walls during 30 days of steady flow conditioning. After the conditioning period, the pipes were flushed to mobilize the sediment deposits. The SSC of water samples collected during the experiments were used to produce translation factors for the online turbidity data. Macroscopic sediment loads were estimated based on the difference between suspended sediments at the inlet and outlet of the pipe loop, while microscopic loads were estimated through the direct observation of particles on pipe wall samples using automated brightfield microscopy. Physical metrics were proposed to adequately represent the sediment load data. Results from the turbidity data analysis produced insights about the impacts of experimental conditions on the SSC translation factors, while microscopy images allowed a detailed assessment of particles deposited on the pipe walls including information about their particle size distribution and dispersion.

Keywords

Discolouration, Iron Oxide Particles, Suspended Sediment Concentration, Brightfield Microscopy.

1 INTRODUCTION

Pipes in drinking water distribution systems (DWDS) commonly experience a chronic material loading [1] that contributes to the accumulation of several contaminants on their pipe walls, including inorganic particles, metals and viable biofilms [2]. This increases the risk of a drinking water contamination event, where a considerable fraction of accumulated materials is quickly mobilized by the bulk flow [3, 4]. This can lead to interactions between the bulk water and the pipe walls that can gradually degrade drinking water quality [5]. The case of material mobilization has historically been the focus of research due to severe water discolouration events that often

surpass established guidelines for potable water turbidity and regulated metals. However, health-related impacts of chronic drinking water degradation are gaining interest because of the prevalence of key contaminants in material deposits (e.g., anti-microbial resistant genes [6, 7]), that have a direct path to the population through drinking water. In either case, water utilities typically have the goal of reducing accumulated material in pipes so as to reduce the risk of contamination in their drinking water systems [4, 8-10].

The first step toward effective material accumulation management is the establishment of a reliable method to quantify the material load, which is already a challenge due to several factors, including: 1) material accumulation is often localized in DWDSs [8, 10]; 2) material composition varies across networks and can include a large range of inorganic and organic elements [3, 4, 11, 12]; 3) accumulation and mobilization phenomena occur over short time scales [11, 13]; 4) the majority of pipes are buried, and a commercialized solution to easily access material deposits is not currently available. Due to these factors, previous approaches to quantify material load in DWDSs have been restricted to the analysis of specific drinking water elements (e.g., turbidity, iron, viable microorganisms), and not fully interchangeable among systems. Historically, the investigation of material accumulation is connected to events of rapid material mobilization commonly known as *discolouration events* [13], where the increase of pipe flow rate provokes the mobilization of materials from the pipe wall. The increase of particulate material in suspension produces the “discoloured” aspect of the water, as a consequence of a decrease in the translucid quality of the water rather than a change in colour. Therefore, the measurement of water turbidity – a common water quality parameter that measures the level of light scatter of fine particles in suspension in *Nephelometric Turbidity Units* (NTU) relative to an established standard in a reference solution [14] – has emerged as the main parameter to quantify material accumulation loads in DWDSs.

Previous research has been focused on turbidity data from flushing operations that were intentionally produced to mobilize materials and clean pipes, from field and laboratory DWDSs [11, 15-18]. These included approaches that considered a pseudo-mass balance of turbidity to estimate material accumulation load in selected systems [19], and the development of discolouration models based on the conservation of turbidity for a wide range of systems [20-22]. Because turbidity is an aesthetic aspect of drinking water, it is also strongly related to customer perception of drinking water quality—something that has motivated its adoption as a key parameter in previous research focused on improving customer satisfaction [15, 16]. Turbidity-based approaches in discolouration research are mostly founded on the argument that the correlation between turbidity and suspended sediment concentration (SSC) remains stable with a consistent particle size distribution (PSD) and particle composition [22, 23]—two parameters that determine their interaction with light. By comparison, other researchers have shown that these conditions are not commonly met in DWDSs, and that the relationship between SSC and turbidity can change substantially among systems and during abrupt changes in operational conditions [11, 24, 25]. Recent research has shown that drinking water PSD is directly connected to the fluid velocity in the pipes and might rapidly change due to the selection of particles that remain in suspension for individual operational conditions—a factor that may drastically alter the relationship between turbidity and SSC [25].

Researchers have also argued that turbidity rather than material load and SSC is a better indicator to manage material accumulation because it directly translates to customer satisfaction [1, 15]. However, drinking water turbidity does not necessarily correspond to water quality, since contaminants might still be present in dissolved form (originating from accumulated materials), or as particles that only make a small contribution to turbidity. Larger particles in the range of 50 μm – 500 μm produce little turbidity due to their low abundance in drinking water [22], but they have an equivalent mass of thousands of fine particles (1 μm – 10 μm). These large particles might still be mobilized during elevated flow events, and it is reasonable to assume that they have

a greater potential to harbour higher contaminant loads than do fine particles while still being small enough to be undetected by customers. In this context, the customer's perception of drinking water quality is biased and insufficient to fully evaluate the risks of contamination events from pipe wall material deposits. Meanwhile, several aspects of the material accumulation problem are still poorly understood, and these are still under-represented by current drinking water quality assessment practices. Nonetheless, there is no proof of a conservation of water turbidity since the changes of PSD are independent of changes of SSC [26]—something that may affect the reliability of long-term models that only consider water turbidity to forecast material accumulation.

The lack of direct assessment of pipe wall conditions and the indirect nature of data acquired through flushing and material mobilization also creates additional challenges to fully understand and quantify material accumulation on drinking water pipes. Turbidity approaches use a short mobilization period (e.g., minutes) at the end of long accumulation periods (e.g., months) to detect a final time-average of material load. In addition, during flushing activities the period of material mobilization from pipe walls is proportional to the flow acceleration period [27] while the water is travelling downstream in the pipes. This produces a mixing of released material from long pipe sections into the same control volume. This tends to decrease the accuracy of material deposits localized through turbidity data and prevents the investigation of distinct attachment along the pipe circumference. By comparison, the processes that account for material accumulation occur over long-time scales (e.g., years) and occur at a microscopic scale at the pipe wall. For this reason, the investigation of the detailed mechanics of material accumulation requires methods of observation of similar time and space scales. Figure 1 contrasts the time and space scales of the processes of material accumulation and mobilization.

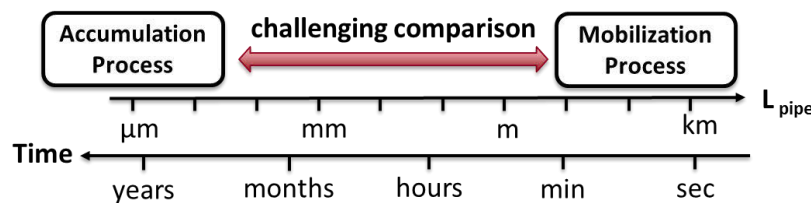


Figure 1 – Comparison of length and time scales of material accumulation and mobilization processes in drinking water pipes.

In this context, previous research has proposed direct methods for assessing biofilms in DWDSs [28, 29] supported by established methods in microbiology that are traditionally used to investigate microorganisms. However, only recent approaches have allowed the direct quantification of inorganic particles on the pipe walls through acquisition of pipe wall samples and direct observation using brightfield microscopy [30]. The method was specifically developed to identify iron oxide particles (the dominant particle that causes in discolouration events [3, 12]) for PVC pipes in a controlled full-scale water distribution laboratory. Using this setup, this paper is focused on comparing two independent pipe wall material quantification approaches based on turbidity and microscopy observations. A controlled experiment was developed in a full-scale PVC laboratory system that partially mimics the conditions of operational DWDSs. The main simplifications of the study were the induced absence of biofilms and the use of stable and homogeneous iron oxide particles in suspension. These simplifications were adopted to facilitate the estimation of particulate deposits in physical mass units.

2 METHODS

2.1 Laboratory experiments

The experiments were realized in the Drinking Water Distribution Laboratory (DWDL) at Queen's University. The DWDL can mimic the hydraulic conditions of real distribution systems in a controlled environment. The laboratory has two independent pipe loops, that are comprised of a water tank with a volume of 3.6 m³, two variable-speed centrifugal pumps (low-flow and high-flow) and 11 coils of IPEX Blue Brute PVC pipe Class 235 (DR18) with an internal diameter 108 mm, and a total length of 193 m. Prior to each experiment, the tanks were cleaned, and the entire system (tanks and loops) was disinfected using sodium hypochlorite at a free chlorine concentration of 20 mg/L with a contact time of 24 h. A unidirectional flushing flow rate of 16 L/s was used to mobilize any remaining material deposits accumulated in the pipes, and the flushed water was discarded and replaced by local drinking water from the City of Kingston. Several water samples were collected at the tap during the experiments and tests showed an average SSC of 60 µg/L with a corresponding turbidity of 0.08 NTU.

The experiment consisted of a 28-day conditioning phase where a fixed volume of water was recirculated at a constant flow rate between the pipe loop and the tank, and a flushing phase where the pipe loop was flushed in 3 sequential steps [31-33]. The hydraulic conditions for each experimental stage are presented in Table 1. A steady conditioning flow rate of 0.6 L s⁻¹ was chosen based on the average flow rate measured in distribution water mains of Canadian DWDSs. The steady flow was used to simplify the interpretation of the particle attachment phenomenon on the pipe walls. The use of a closed system volume (no water renewal) was chosen to make it possible to perform a mass balance on the material entering and leaving the pipe loop. In doing so, it was possible to quantify the amount of particulate mass accumulated in the pipe loop and the amount of mass mobilized in each flushing stage. The closed volume also assisted in preventing biofilm formation due the limited source of nutrients in the initial drinking water. In addition, a free chlorine concentration of approximately 0.2 mg/L was maintained through weekly addition of sodium hypochlorite to the system based on weekly monitoring and an empirical decay curve.

The experiment was completed in duplicate using the North and South pipe loops, where the water was inoculated with 1 mg L⁻¹ of particulate iron oxides to encourage the formation of iron oxide deposits on the pipe wall. The SSC value is substantially higher than common values for drinking water but chosen to amplify the material attachment phenomena and facilitate its detection. During the experiments, both pipe loops were subject to the same hydraulic, environmental, and physico-chemical conditions to obtain a duplicate set of data. A chemical grade of red iron oxide powder from Alpha Chemicals, with a composition of 82% of Iron(III) oxide – Fe₂O₃ was chosen to be the source of particles for the experiments due to its stable particulate form and insolubility in water. The powder particle size distribution analysis through laser diffraction showed a predominance of small sizes, with 10% of particles smaller than 0.8 µm, a median particle diameter (D₅₀) of 6.3 µm, and 20% of particles larger than 10.8 µm. A stable water conductivity and pH measured through the experiments suggested that little changes in the water chemistry occurred during all the experiments.

To start the experiment, the iron oxide particles were added as a single load into the tanks. This method was preferred to a progressive addition of particles mostly due to the practical challenges of maintaining a consistent concentration in the system due to the lack of control of particles mixing in the tanks. After the inoculation, the pipe loops were operated at a steady, conditioning flow rate (Table 1) for 28 days to allow particles to adhere to the pipe walls. Following the conditioning phase and prior to the flushing phase, the tank and the pipes on the suction and discharge sides of the pumps were pre-flushed to remove whatever iron oxide particles may have accumulated in these sections and to prevent reintroducing materials from these components into the pipe loops during the flushing steps of the experiment. In the flushing stage, three unidirectional flushing steps were performed in sequence in each pipe loop to mobilize material deposits from the pipe walls at different WSS levels (Table 1). During the flushing steps, the pipe

loops were operated in a non-recirculatory manner, where the water was discarded at the outlet of the pipe loop instead of re-entering the tank.

During the experiments, the flow rate and turbidity were continuously monitored at 1 Hz in each pipe loop with two Sierra InnoVaSonic® 205i Ultrasonic Flow Meters ($\pm 0.5\%$) and two online Hach TU5300sc turbidimeters (± 0.01 NTU). The turbidimeters were configured to monitor the water at the pipe loop inlet and at the pipe loop outlet. The TU5300sc turbidimeters were specifically chosen for use in the DWDL due to their small flow cell of only 10 mL. However, because the sensor uses a “flow-through approach” and required the extraction of the water from the system, a special installation scheme was needed to achieve a reliable operation and prevent the depletion of the finite water of the system (Figure 2a). First, unique plastic sampling ports that collect water from the centreline of the pipes was developed using 3D printing technology (Figure 2b). The aim of this bespoke sampling device was to achieve an approximate isokinetic sampling condition – same fluid velocity entrance at the collection tubing as the local flow velocity – to reduce sampling errors associated with the inertia of the suspended particles. Second, a modification of the sensor operation was realized by the addition of a small plastic centrifugal pump in the tubing downstream of the sensor location that pumped the water back into the pipe loop (Figure 2a). These modifications guaranteed that the required flow rate for the sensor operation was consistent and maintained regardless of the hydraulic conditions in the pipes. In addition, the installation of the small centrifugal pump downstream of the sensor prevented possible impacts of this pump to the sensor readings. Several preliminary tests using multiple flow configurations and controlled concentrations of similar iron oxide particles demonstrated that turbidity readings were very sensitive to hydraulic conditions of the sensor tubing. These justified the substantial efforts placed to guarantee a consistent operation of the turbidity sensors during the experiments.

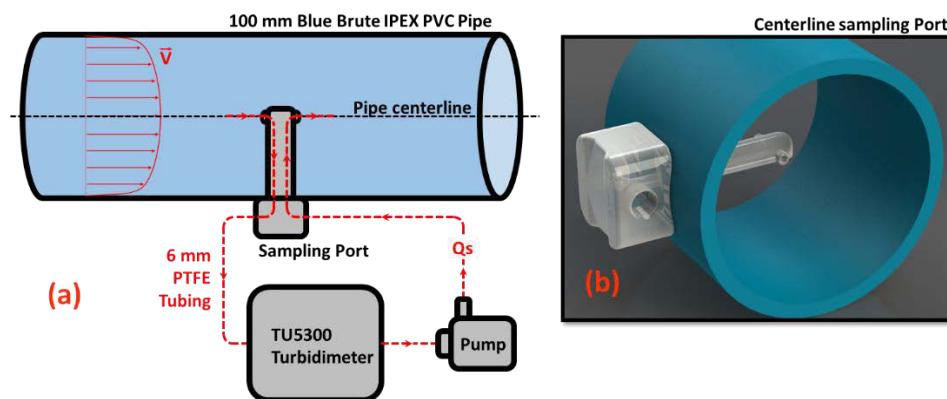


Figure 2 – a) Special scheme for the installation of turbidimeters in the pipe loop; b) rendered model of the 3D printed sampling ports to collect/return water at the centreline of the pipes.

A similar approach was used to collect grab water samples from the centreline of pipes during the experiments for measuring the bulk water SSC. 3D printed sampling ports designed to maintain isokinetic conditions were produced for low- and high-sampling flow rates. Low-flow ports were installed at the inlet and outlet positions of the pipe loop, while a single high-flow sampling port was installed at the outlet only. The low-flow ports were mainly used to collect samples during the conditioning phase of the experiments under stable conditions. By contrast, the high-flow sampling ports were used to collect large sample volumes during short periods of the flushing phases under potentially variable SSC conditions.

A unique pipe wall coupon sampling system [30] was used to directly monitor material deposits on the internal surface of the PVC pipes. The coupon sampling system was developed by cutting out circular PVC coupons from the native PVC pipe and mounting them on a 3D-printed coupon support base. The circular PVC coupon and support base were designed to be inserted in custom,

pre-drilled holes and affixed with a metal clamp to prevent leakage when the pipe loop was pressurized. The coupon system allows for a precise surface alignment of the internal surface of the coupon with the surrounding pipe wall surface that is in the range of ± 0.1 mm. This guarantees that the internal surface of the coupon will experience the same flow conditions as does the surrounding pipe wall without disturbing the local velocity profile in the viscous sub-layer region (VSL). Only coupons installed in the invert positions were used for the material quantification, since no particles were found in the obvert and springline positions [34]. During the conditioning phase of the experiments, pipe wall coupons in the invert pipe position were acquired every 7 days to assess the pipe wall conditions. During the flushing phase, invert pipe wall coupon samples were acquired between the flushing steps to assess the pipe wall conditions.

2.2 Material estimation based on turbidity data

The continuous, high-frequency monitoring of turbidity at the inlet and the outlet of the pipe loops was used to estimate changes in the SSC of the bulk water that was sequentially used to calculate the transport of iron oxide particles from the bulk water to the system pipe wall and tank. For this, turbidity data was transformed to continuous SSC data through calibration coefficients (κ ($\text{mg L}^{-1} \text{NTU}^{-1}$)) obtained from valid SSC samples that were also complemented by previous experimental data under similar conditions [34]. Turbidity values for the calibration were obtained directly from the pipe loop – from the correspondent control volume from where the SSC samples were collected – rather than values from portable turbidimeters. For the flushing stage of the experiment, SSC sample data was regressed against turbidity data to estimate a constant calibration coefficient. However, for the conditioning stage of the experiment, a decrease of the calibration coefficient was observed over time. To cope with this, a *calibration coefficient curve* ($\kappa(t)$) that varied as function of time was used to transform the turbidity data to SSC values. The calibration coefficients were used to transform the turbidity data series ($T(\text{NTU})$) to SSC ($C(\text{mg L}^{-1})$) using Equation 1.

$$C = \kappa \times T \quad (1)$$

Following this, the flux of suspended sediments (Q_{SS} (mg s^{-1})) through the turbidity monitoring sections was calculated using Equation 2 as the product of the measured flow rate in the pipes (Q (L s^{-1})) and the SSC (C (mg L^{-1})). The total accumulated load of iron oxide particles attached to the pipe wall (M_{PW} (mg)) in each experimental stage was estimated by integrating the difference in suspended material flux at the inlet and outlet of the pipe loop length between the turbidimeters over time (Equation 3).

$$Q_{SS} = Q \times C \quad (2)$$

$$M_{PW} = \int_t (Q_{SS, in} - Q_{SS, out}) dt \quad (3)$$

where t = period of time over which suspended materials are deposited on pipe wall (seconds); $Q_{SS, in}$, $Q_{SS, out}$ = flux of suspended sediments estimated from turbidity data measured at the inlet and outlet of the pipe loop. The duration of the inoculation stage was 180 minutes (corresponded to 3 complete turn-overs of the pipe loop volume), and the conditioning stage lasted for 30 days. The period that corresponds to the passage of 3 pipe-loop volumes was used for each flushing step.

The material accumulated in the tanks (M_{Tank} (mg)) was calculated using Equation 4 as the difference between the total mass of iron oxide particles initially added (M_{Fe} (mg)), the material load estimation of particles attached to the pipe wall (M_{PW} (mg)), and the material mass that remained in suspension (M_{SSC} (mg)). The load of material in suspension (M_{SSC} (mg)) was estimated

with Equation 5 by multiplying the instantaneous SSC (C (mg L⁻¹)) at the inlet position by the total volume of the water (V_T (L)).

$$M_{Tank} = M_{Fe} - M_{PW} - M_{SSC} \quad (4)$$

$$M_{SSC} = C \times V_T \quad (5)$$

Equations 1 – 5 were used to estimate the accumulation of iron oxide particles on the internal surface of the pipe loops during the inoculation and conditioning phases (positive material load), and the mobilization of iron oxide particles from the pipe surface after each flushing step (negative material load). Before the pipe flushing stage, the tank and pump side of the system was pre-flushed at the maximum flow rate, and all particles that could be mobilized were discarded with the renewal of the tank water. Because of that, and due to the non-recirculating strategy adopted during the pipe flushing stage, all material load entering in the pipe loop during the flushing stage was assumed to be negligible.

2.3 Material estimation based on microscopy data

Pipe wall samples were retrieved from a middle section of the pipe loop during the conditioning and flushing phases of the experiment and were processed according to the monitoring scheme developed by the authors [35]. Pipe wall samples collected from the invert pipe positions were used in this study. All samples were collected within a pipe length of 20 m located approximately 100 m from the inlet of the pipe loop and assumed to be invariant with the pipe length. The pipe wall samples were carefully unmounted from their 3D-printed support base and air dried at 30°C for 24 h before they were imaged with a brightfield microscope. Four samples and up to 44 fields of view (FOV) of each coupon sample were captured per sampling cycle using an automated upright microscope Nikon Eclipse Ni-E in brightfield mode and a CFI60 Super Plan Fluor ELWD 40x objective lens. The final images were used to characterize the attachment of iron oxide particles on the pipe wall and their adherence to the PVC pipe substrate by means of a MATLAB image-processing script and a quantitative particle analysis. The image-processing script was used to detect individual iron oxide particles by differentiating them from the PVC pipe substrate and calculating their individual coverage area (μm^2). The multiple FOVs captured from each coupon sample were used to calculate the particle coverage area mean and standard deviation.

The microscopic material load M_{FOV} (mg) per field of view area was calculated by following a number of steps. First, the total volume of iron oxide particles detected in each FOV (V_P (μm^3)) was estimated using Equation 6 by multiplying the mean particle cross section area (A_P (μm^2)) by the average particle diameter (d_P (μm)) that was determined to be 1.5 μm from the analysis of a previously generated dataset [34]. For the total volume calculation, it was further assumed that the particles were spherical and therefore a volume reduction factor of 0.52 (ratio between the volume of a sphere imprint into a cube) was applied (Equation 6). In comparison to Braga and Filion [34], the new method proposed here aims to improve the previous calculation of particle volume through its equivalent diameter. In addition, the new approach is also supported by data from recent experiments [25], which suggests that only small particles (< 5 μm) should be able to reach the coupon sections under the hydraulic conditions tested. An estimate of the average iron oxide particle mass per FOV (M_{FOV} (mg)) was calculated by multiplying a constant iron oxide density (ρ) of 5.24 mg cm⁻³ by the total volume (Equation 7), and the average iron oxide area density per FOV (S_{FOV} (mg m⁻²)) was calculated by dividing M_{FOV} (mg) by the microscope image FOV area (A_{FOV}) of 0.071 $\times 10^{-6}$ m² (Equation 8).

$$V_P = 0.52 \times A_P \times d_P \quad (6)$$

$$M_{FOV} = \rho \cdot V_P \quad (7)$$

$$S_{FOV} = \frac{M_{FOV}}{A_{FOV}} \quad (8)$$

In order to calculate the total material load on the pipe loop using the microscopy data was required to extrapolate the average iron oxide area density per FOV to the total area covered by particles, while experimental evidence from the experiments suggest that particle attachment occurred only in the invert region of the pipe circumference [34]. A corrected surface area (A_{Fe} (m²)) corresponding to the area occupied by particles, was estimated from the total pipe area (A_T (m²)) using Equation 9. The correction factor α corresponds to the fraction of the pipe circumference where materials were deposited. The observation of inner pipe walls after preliminary experiments suggested that most of the material deposits had accumulated on the invert region of the pipes. Therefore, in this study it was assumed $\alpha = 1/16$ (angle of 11.25° for each side from the pipe invert). The average iron oxide area density per FOV (S_{FOV} (mg m⁻²)) was also assumed to represent the average area density in the invert region of the whole pipe loop length.

$$A_{Fe} = \alpha A_T \quad (9)$$

Finally, the estimation of the total material load accumulated on the pipe wall based on the microscopy data (M_{PW_mic} (mg)) was calculated using Equation 10 by multiplying the average iron oxide area density per FOV (S_{FOV} (mg m⁻²)) and the corrected surface area (A_{Fe} (m²)).

$$M_{PW_mic} = S_{FOV} \times A_{Fe} \quad (10)$$

3 RESULTS & DISCUSSION

Figure 3 presents the relationship between SSC and turbidity used for the estimation of particulate material transport in the experiments. Figure 3a shows the decay of the linear transformation coefficient κ along the conditioning stage period of the experiment, and the empirical equation used to interpolate the data. After approximately 20 days of conditioning, there was no more measurable fractions of the SSC in the bulk water, but there was still a detectable level of turbidity caused by the iron oxide particles that resulted in a coefficient $\kappa = 0$. The decrease in the coefficient over time was likely caused by the more rapid attachment of larger particle fractions to the pipe wall during the experiment— a phenomenon that was also observed in Braga and Filion [25]. But in this case the effect was hastened by the passage of the recirculating water through the tank region where the flow is laminar and insufficient to maintain particles in suspension and causes the particles to settle more rapidly. The disproportional reduction in larger particle fractions relative to the fine fractions likely changed the PSD of the particles in suspension which in turn had an impact on the relationship between turbidity and SSC [14].

By comparison, Figure 3b shows that an adjusted constant coefficient $\kappa = 0.35$ mg L⁻¹ NTU⁻¹ fit the sample data well during the flushing stage of the experiments. The goodness-of-fit adjustment of the calibration coefficient indicate that particle suspension from all flushing steps had a similar PSD. This suggests that all flushing operations mobilized particles of similar sizes. This observation agrees with observations from previous experiments that showed that a narrow range of fine particle sizes are selected to populate the downstream sections of the pipe loop, while larger fractions are rapidly lost in the initial pipe lengths [25]. The SSC samples collected during the flushing stage of the present experiment corresponded to the middle section of the pipe loop (same as the coupon sections) and did not incorporate material from the initial pipe sections.

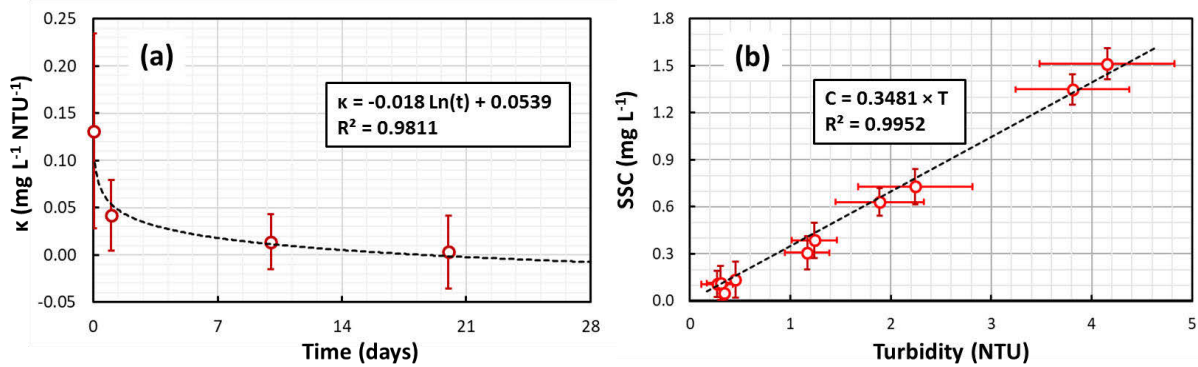


Figure 3 – a) Decay of the calibration coefficient κ along the conditioning phase of the experiment; b) linear SSC vs. turbidity relationship for the flushing phase of the experiments.

The results of the SSC and estimations of iron oxide particle accumulation on the pipe wall using the turbidity data for the conditioning phase of the experiment are presented in Figure 4. In particular, Figure 4a shows the SSC and the iron oxide particle accumulation on the pipe wall in the first 3 hours following the particle inoculation. The data here suggests that a rapid accumulation occurred in the first hour during the first passage of the particle plume through the pipes. This observation is likely explained by the entrainment of large particles ($>6 \mu\text{m}$) from the tank and into the loop; these large particles were likely rapidly deposited in the initial sections of the pipe loop [25].

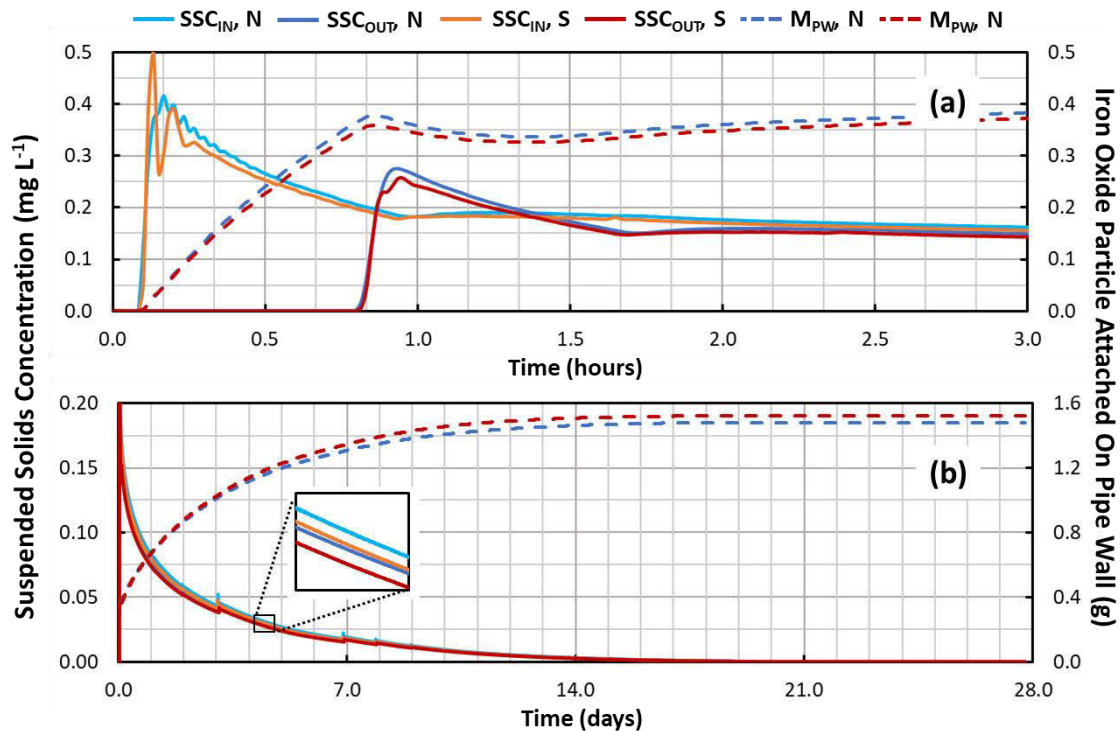


Figure 4 - SSC and iron oxide particle attached on pipe wall for the the conditioning phase of the experiment after a) 3 hours, and b) 28 days.

Once the larger particles settled to the bottom of the tanks and onto the internal surface of the pipes, the concentration of particles held in suspension decreased at a lower rate (Figure 4b). Particle accumulation on the pipe wall progressively increased based on the small difference between the inlet SSC and the outlet SSC as shown in Figure 4b. Despite this, the accumulation

rate decreased over time and reached a value of zero after 20 days of conditioning when the SSC levels measured in the bulk water fell to zero. Approximately 1.5 g of iron oxide particles were deposited in the pipe loop at the end of the conditioning phase.

Results for the SSC and particle mobilization during the flushing phase of the experiments are presented in Figure 5. The first flushing step (FS1 – Figure 5a) mobilized the larger particles with a mobilization of 0.8 g for both pipe loops (72% of total mobilized load). The second flushing step (FS2 – Figure 5b) also mobilized a substantial amount of material (21%). Also, the particles that remained attached to the pipe wall had a shear strength higher than the self-cleaning level of 1.2 Pa (WSS of the FS1) previously proposed [17]. Lastly, the third flushing step (FS3 – Figure 5c) showed that a small fraction of particles (7%) was able to resist a shear stress of 3.0 Pa (WSS of the FS2); these particles however were mobilized at 5.0 Pa. However, it is noted that very low turbidity levels likely resulted in higher proportional errors in the estimation of the turbidity profile during the third flushing step FS3.

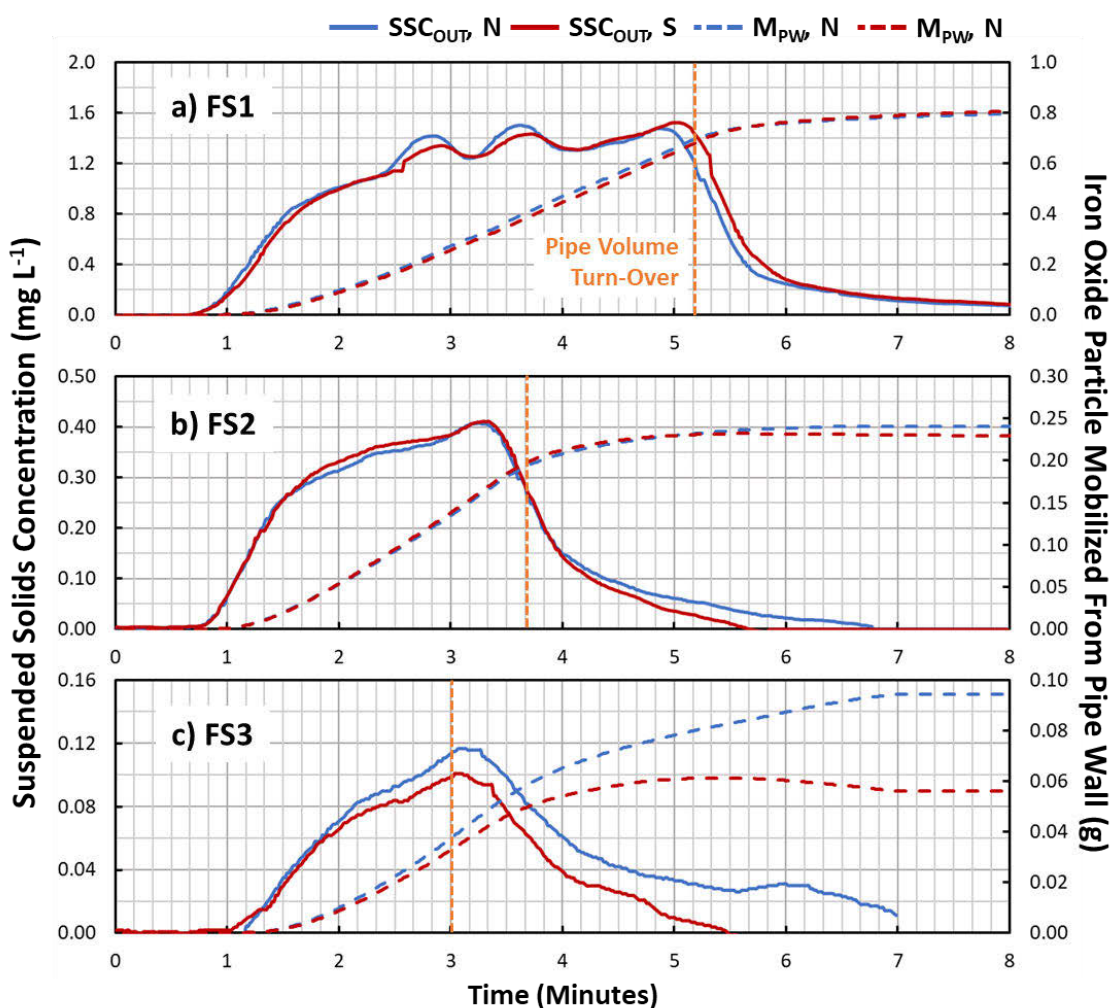


Figure 5 - SSC and iron oxide particles mobilized from the pipe wall for the the three flushing steps (FS1, FS2 and FS3) of the flushing phase of the experiment.

The SSC profiles of all flushing steps were similar and showed a slight tendency to reach peak turbidity at the single pipe volume turn-over point (Figure 5). This suggests that particle shear strength was independent of the pipe length, but that a higher accumulation load occurred in the initial sections of the pipe and progressively decreased along the pipe length. Approximately 1.1 g of iron oxide particles were mobilized from the pipe wall during the flushing phase.

The location of the iron oxide particles in all phases of the experiment was estimated by way of a mass balance analysis and the results are shown in Figure 6. In the conditioning phase, from an initial total mass of 4.4 g of iron oxide particles added to the system, only 19% remained in the bulk water 3 h after the inoculation, while 73% were estimated to be deposited in the tanks and 9% were attached to the pipe loop. The results suggest that the bulk fraction was mostly transferred to the pipe loop rather than to the tanks, while the material accumulated in the tank was reduced from 73% to 67% during the conditioning phase. This error is likely caused by an underestimation of the initial bulk water SSC, which was calibrated mostly through SSC samples collected from the turbidity positions at the pipe loop – a position that most large particles never reached. However, the error affected the early estimations of the material deposited in the tanks, since the fraction of particles accumulated in the pipe wall was estimated based on a SSC difference. In this case, the error in the initial bulk water SSC was resolved by the SSC difference operation. The only error remaining in the pipe wall load estimation arose from a longer period for the coefficient κ to reach zero, which in this case had a negligible contribution to the final load.

In the case of the flushing phase (right side of Figure 6), an initial load of 1.5 g of iron oxide particles accumulated on the pipe wall was progressively mobilized through the three flushing steps (FS1, FS2 and FS3). The flushing step FS1 mobilized 54% of the estimated attached particles, the FS2 step mobilized 16% and the FS3 step mobilized 5%, while an estimated fraction of 25% of the initial particles remained attached to the pipe walls. These correspond to 9% of the initial fraction of particles inoculated in the system.

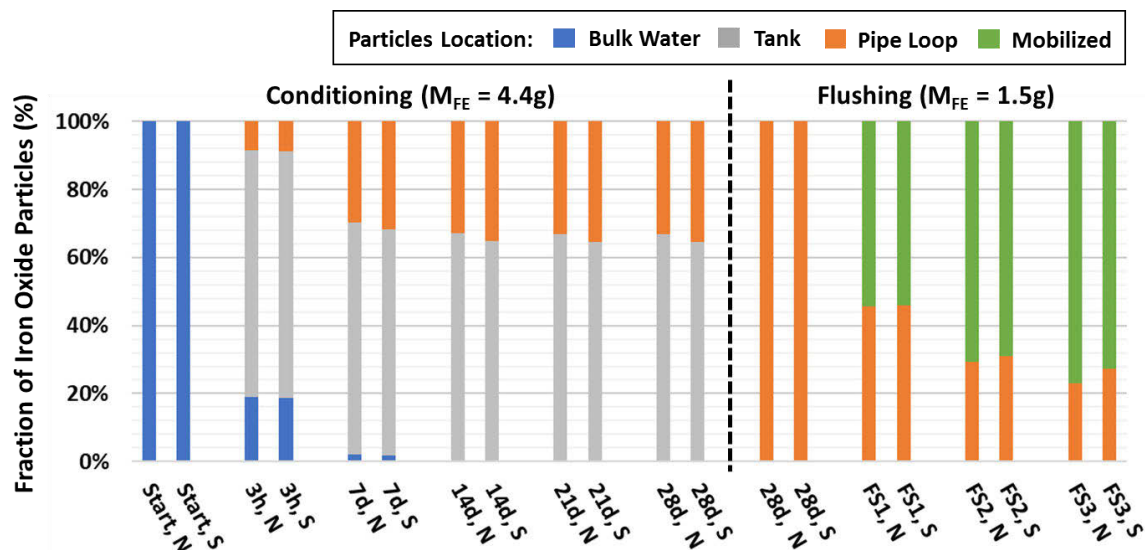


Figure 6 - Location of the iron oxide particles introduced in the pipe loop at various stages of the experiment (estimated through a mass balance analysis). "Tank" denotes the particles that settled to the bottom of the tank, "Bulk Water" denotes the particles held in suspension in the pipe loop, "Pipe Loop" denotes the particles attached to the internal surface of the pipe wall, and "Mobilized" denotes the particles mobilized during the flushing steps. It is noted that at the beginning of the flushing phase of the experiment (after 28 d), 1.5g of particles were adhered to the pipe wall and this mass is represented as 100% in this figure.

The results of the comparison between the turbidity and microscopy approaches to estimate the mass of particles attached to the pipe wall are shown in Figure 7 for each stage of the experiment where pipe wall samples were collected. During the conditioning phase, the microscopy estimations were substantially smaller than the turbidity-based method. The discrepancy may be explained by results from previous experiments that suggested that particle accumulation occurs to a greater extent in the upstream sections of the pipe loop near the inlet [25] and to a lesser extent in the downstream sections near the outlet. Because pipe wall coupons were only available in the middle section of the pipes, their data extrapolation to the whole pipe loop largely

underestimates deposits from initial pipe sections. By comparison, results for the flushing phase shows good agreement between both methods, confirming the decrease in particles on the pipe loop along the three flushing steps and a remaining fraction on the pipe wall even after the third flushing step FS3.

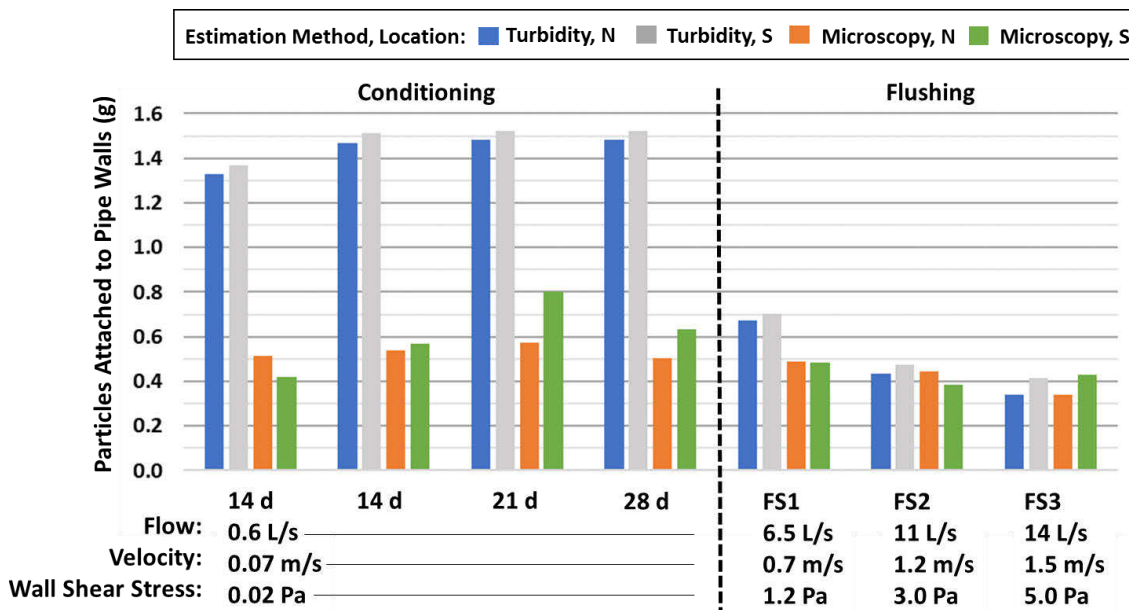


Figure 7 – Comparison of turbidity and microscopy approaches to estimate the mass of particles attached to the pipe wall for the conditioning and flushing stages of the experiment.

Lastly, the results of the microscopy approach to estimate the mass of particles attached to the pipe wall during the conditioning phase are shown in Figure 8. Particle accumulation followed a linear trend over time and suggested that particles accumulated on the pipe wall at the rate of 6.3 mg day^{-1} during the conditioning phase, while an approximate load of 0.46 g was initially deposited during the first passage of the particle plume. These estimations correspond only to particle fractions observed on the coupon wall samples, but they support the hypothesis that a small attachment rate of fine particles does prevail in suspension for longer periods [25]. It is worth noting that the error bars only considered the variation of material estimation across multiple FOVs of microscopic images, and do not include the extrapolation error of the data for the entire pipe area.

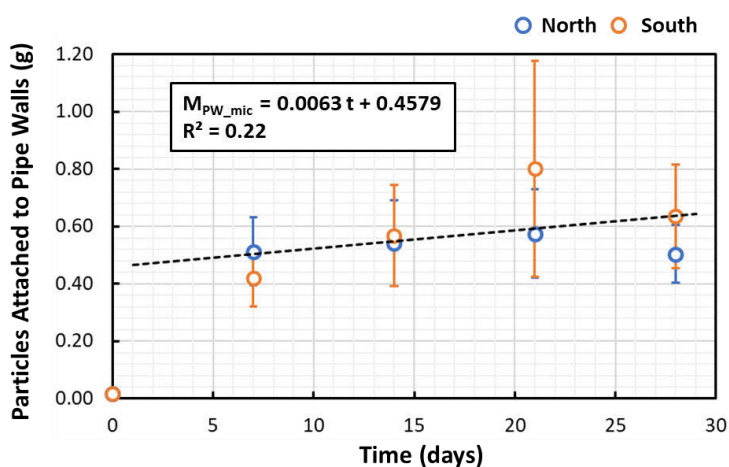


Figure 8 – Estimations of particle attachment with the microscopy approach for the conditioning phase of the experiment.

4 CONCLUSION

This paper presented a turbidity approach and a direct microscopy approach to quantify the accumulation of iron oxide particles in a full-scale PVC pipe loop facility that mimics an operational DWDS. Results showed that particle accumulation on the pipe walls ended after 20 days of conditioning. At this time, approximately 30% of the material introduced into the loop had accumulated on the pipe wall and the rest accumulated in the system tank. Microscopy results showed that the accumulation of particles on coupon samples was 3 times smaller during the conditioning phase due to the fact that the bulk of particles were deposited in the initial sections of the pipes, away from pipe wall samples. However, material estimations after the three flushing steps showed good agreement between the turbidity and microscopy data, suggesting the larger fractions causing earlier discrepancy were mobilized in the first flushing step. Approximately 8% of the particles introduced into the pipe loop remained in the pipes after the last flushing step with a WSS of 5 Pa.

The efforts made to estimate material loads in physical units were fundamental to the mass balance approach used in the experiments, and for the direct comparison of the turbidity and microscopy quantification methods. The assumption of a constant relationship between SSC and turbidity for all stages of the experiment would have created a strong discrepancy in the results. Specifically, a large fraction of particles added to the system that did not contribute to turbidity would not have been quantified. The proposed methods still have considerable sources of errors, but these are likely smaller than errors incurred by using uncalibrated turbidity data or porting coefficients from systems with different or unknown particles characteristics.

Future research will aim to better assess drinking water SSC and PSD. This will have the potential to reduce errors of turbidity data usage for material accumulation estimations, while the evolution of the microscopic assessment methods has also potential to contribute to complementary data. New studies are also needed to examine the occurrence of biofilms and possible precipitation of particles as sources of material accumulation at the pipe wall, as well as additional pipe wall materials and other operational conditions such as variable flow.

5 REFERENCES

- [1] I. Sunny, P. S. Husband, and J. B. Boxall, "Impact of hydraulic interventions on chronic and acute material loading and discoloration risk in drinking water distribution systems," *Water Research*, vol. 169, p. 115224, 2020/02/01/ 2020, doi: <https://doi.org/10.1016/j.watres.2019.115224>.
- [2] G. Liu et al., "Hotspots for selected metal elements and microbes accumulation and the corresponding water quality deterioration potential in an unchlorinated drinking water distribution system," *Water Res*, vol. 124, pp. 435-445, Nov 1 2017, doi: [10.1016/j.watres.2017.08.002](https://doi.org/10.1016/j.watres.2017.08.002).
- [3] A. Seth, R. Bachmann, J. Boxall, A. Saul, and R. Edyvean, "Characterisation of materials causing discoloration in potable water systems," *Water Science and Technology*, vol. 49, no. 2, pp. 27-32, 2004, doi: [10.2166/wst.2004.0080](https://doi.org/10.2166/wst.2004.0080).
- [4] A. Carrière, V. Gauthier, R. Desjardins, and B. Barbeau, "Evaluation of loose deposits in distribution systems through: unidirectional flushing," *Journal - American Water Works Association*, vol. 97, no. 9, pp. 82-92, 2005, doi: [10.1002/j.1551-8833.2005.tb07474.x](https://doi.org/10.1002/j.1551-8833.2005.tb07474.x).
- [5] S. Triantafyllidou, D. A. Lytle, A. S. C. Chen, L. Wang, C. Muhlen, and T. J. Sorg, "Patterns of arsenic release in drinking water distribution systems," *AWWA Water Science*, vol. 1, no. 4, p. e1149, 2019, doi: <https://doi.org/10.1002/aws2.1149>.
- [6] V. Rilstone, L. Vignale, J. Craddock, A. Cushing, Y. Filion, and P. Champagne, "The role of antibiotics and heavy metals on the development, promotion, and dissemination of antimicrobial resistance in drinking water biofilms," *Chemosphere*, vol. 282, p. 131048, Nov 2021, doi: [10.1016/j.chemosphere.2021.131048](https://doi.org/10.1016/j.chemosphere.2021.131048).
- [7] L. K. Kimbell et al., "Cast iron drinking water pipe biofilms support diverse microbial communities containing antibiotic resistance genes, metal resistance genes, and class 1 integrons," *Environmental Science:*

- Water Research & Technology, 10.1039/D0EW01059F vol. 7, no. 3, pp. 584-598, 2021, doi: 10.1039/D0EW01059F.
- [8] B. Barbeau, K. Julienne, A. Carriere, and V. Gauthier, "Dead-end flushing of a distribution system: Short and long-term effects on water quality," *Journal of Water Supply: Research and Technology-Aqua*, vol. 54, no. 6, pp. 371-383, 2005, doi: 10.2166/aqua.2005.0035.
- [9] M. J. Lehtola, T. K. Nissinen, I. T. Miettinen, P. J. Martikainen, and T. Vartiainen, "Removal of soft deposits from the distribution system improves the drinking water quality," *Water Res*, vol. 38, no. 3, pp. 601-10, Feb 2004, doi: 10.1016/j.watres.2003.10.054.
- [10] O. M. Zacheus, M. J. Lehtola, L. K. Korhonen, and P. J. Martikainen, "Soft deposits, the key site for microbial growth in drinking water distribution networks," *Water Research*, vol. 35, no. 7, pp. 1757-1765, 2001/05/01/2001, doi: [https://doi.org/10.1016/S0043-1354\(00\)00431-0](https://doi.org/10.1016/S0043-1354(00)00431-0).
- [11] J. H. Vreeburg, D. Schippers, J. Q. Verberk, and J. C. van Dijk, "Impact of particles on sediment accumulation in a drinking water distribution system," *Water Res*, vol. 42, no. 16, pp. 4233-42, Oct 2008, doi: 10.1016/j.watres.2008.05.024.
- [12] A. Mussared, R. Fabris, J. Vreeburg, J. Jelbart, and M. Drikas, "The origin and risks associated with loose deposits in a drinking water distribution system," *Water Supply*, vol. 19, no. 1, pp. 291-302, 2019, doi: 10.2166/ws.2018.073.
- [13] J. H. Vreeburg and J. B. Boxall, "Discolouration in potable water distribution systems: a review," *Water Res*, vol. 41, no. 3, pp. 519-29, Feb 2007, doi: 10.1016/j.watres.2006.09.028.
- [14] B. G. B. Kitchener, J. Wainwright, and A. J. Parsons, "A review of the principles of turbidity measurement," *Progress in Physical Geography: Earth and Environment*, vol. 41, no. 5, pp. 620-642, 2017, doi: 10.1177/0309133317726540.
- [15] H. Armand, I. I. Stoianov, and N. J. D. Graham, "A holistic assessment of discolouration processes in water distribution networks," *Urban Water Journal*, vol. 14, no. 3, pp. 263-277, 2015, doi: 10.1080/1573062x.2015.1111912.
- [16] D. M. Cook and J. B. Boxall, "Discoloration Material Accumulation in Water Distribution Systems," *Journal of Pipeline Systems Engineering and Practice*, vol. 2, no. 4, pp. 113-122, 2011, doi: 10.1061/(asce)ps.1949-1204.0000083.
- [17] P. S. Husband and J. B. Boxall, "Asset deterioration and discolouration in water distribution systems," *Water Res*, vol. 45, no. 1, pp. 113-24, Jan 2011, doi: 10.1016/j.watres.2010.08.021.
- [18] S. Husband and J. B. Boxall, "Field Studies of Discoloration in Water Distribution Systems: Model Verification and Practical Implications," *Journal of Environmental Engineering*, vol. 136, no. 1, pp. 86-94, 2010, doi: 10.1061/(asce)ee.1943-7870.0000115.
- [19] E. J. M. Blokker and P. G. Schaap, "Particle Accumulation Rate of Drinking Water Distribution Systems Determined by Incoming Turbidity," *Procedia Engineering*, vol. 119, pp. 290-298, 2015, doi: 10.1016/j.proeng.2015.08.888.
- [20] J. van Summeren and M. Blokker, "Modeling particle transport and discoloration risk in drinking water distribution networks," *Drinking Water Engineering and Science*, vol. 10, no. 2, pp. 99-107, 2017, doi: 10.5194/dwes-10-99-2017.
- [21] W. R. Furnass, R. P. Collins, P. S. Husband, R. L. Sharpe, S. R. Mounce, and J. B. Boxall, "Modelling both the continual erosion and regeneration of discolouration material in drinking water distribution systems," *Water Supply*, vol. 14, no. 1, pp. 81-90, 2014, doi: 10.2166/ws.2013.176.
- [22] J. B. Boxall and A. J. Saul, "Modeling Discoloration in Potable Water Distribution Systems," *Journal of Environmental Engineering*, vol. 131, no. 5, pp. 716-725, 2005, doi: doi:10.1061/(ASCE)0733-9372(2005)131:5(716).
- [23] J. B. Boxall, A. J. Saul, J. D. Gunstead, and N. Dewis, "Regeneration of Discolouration in Distribution Systems," in *World Water & Environmental Resources Congress 2003*, 2003, pp. 1-9.
- [24] F. Pourcel, S. Duchesne, and M. Ouellet, "Evolution of the relationship between total suspended solids concentration and turbidity during flushing sequences of water pipes," *Journal of Water Supply: Research and Technology-Aqua*, vol. 69, no. 4, pp. 376-386, 2020, doi: 10.2166/aqua.2020.127.
- [25] A. S. Braga and Y. Fillion, "The interplay of suspended sediment concentration, particle size and fluid velocity on the rapid deposition of suspended iron oxide particles in PVC drinking water pipes," *Water Research X*, vol. 15, p. 100143, 2022/05/01/ 2022, doi: <https://doi.org/10.1016/j.wroa.2022.100143>.

- [26] T. Walski, K. Minnich, C. Sherman, L. Strause, and B. Whitman, "Can There be a Law of Conservation of Turbidity," *Procedia Engineering*, vol. 186, pp. 372-379, 2017, doi: 10.1016/j.proeng.2017.03.233.
- [27] A. S. Braga, R. Saulnier, Y. Filion, and A. Cushing, "Dynamics of material detachment from drinking water pipes under flushing conditions in a full-scale drinking water laboratory system," *Urban Water Journal*, vol. 17, no. 8, pp. 745-753, 2020, doi: 10.1080/1573062x.2020.1800759.
- [28] K. E. Fish et al., "Characterisation of the physical composition and microbial community structure of biofilms within a model full-scale drinking water distribution system," *PLoS One*, vol. 10, no. 2, p. e0115824, 2015, doi: 10.1371/journal.pone.0115824.
- [29] P. Deines, R. Sekar, P. S. Husband, J. B. Boxall, A. M. Osborn, and C. A. Biggs, "A new coupon design for simultaneous analysis of in situ microbial biofilm formation and community structure in drinking water distribution systems," *Appl Microbiol Biotechnol*, vol. 87, no. 2, pp. 749-56, Jun 2010, doi: 10.1007/s00253-010-2510-x.
- [30] A. S. Braga and Y. Filion, "A novel monitoring scheme to detect iron oxide particle deposits on the internal surface of PVC drinking water pipes," *Environmental Science: Water Research & Technology*, 10.1039/D1EW00614B vol. 7, no. 11, pp. 2116-2128, 2021, doi: 10.1039/D1EW00614B.
- [31] W. Furnass, I. Douterelo, R. Collins, S. Mounce, and J. Boxall, "Controlled, Realistic-scale, Experimental Study of How the Quantity and Erodibility of Discolouration Material Varies with Shear Strength," *Procedia Engineering*, vol. 89, pp. 135-142, 2014, doi: 10.1016/j.proeng.2014.11.169.
- [32] R. L. Sharpe, C. J. Smith, J. B. Boxall, and C. A. Biggs, "Pilot Scale Laboratory Investigations into the Impact of Steady State Conditioning Flow on Potable Water Discolouration," in *Water Distribution Systems Analysis 2010, 2011*, pp. 494-506.
- [33] P. S. Husband, J. B. Boxall, and A. J. Saul, "Laboratory studies investigating the processes leading to discolouration in water distribution networks," *Water Res*, vol. 42, no. 16, pp. 4309-18, Oct 2008, doi: 10.1016/j.watres.2008.07.026.
- [34] A. S. Braga and Y. Filion, "Initial stages of particulate iron oxide attachment on drinking water PVC pipes characterized by turbidity data and brightfield microscopy from a full-scale laboratory," *Environmental Science: Water Research & Technology*, 10.1039/D2EW00010E 2022, doi: 10.1039/D2EW00010E.
- [35] A. S. Braga and Y. Filion, "A novel monitoring scheme to detect iron oxide particle deposits on the internal surface of PVC drinking water pipes," *Environmental Science: Water Research & Technology*, 2021, doi: 10.1039/d1ew00614b.